Microwave-Assisted Solvothermal Synthesis of UiO-66-NH$_2$ and Its Catalytic Performance toward the Hydrolysis of a Nerve Agent Simulant

Zenghui Zhang, Cheng-An Tao * , **Jie Zhao, Fang Wang, Jian Huang and Jianfang Wang ***

College of Liberal Arts and Science, National University of Defense Technology, Changsha 410073, China; zhangch@nudt.edu.cn (Z.Z.); zhaojie15@nudt.edu.cn (J.Z.); Wangf@nudt.edu.cn (F.W.); huangjian2015@nudt.edu.cn (J.H.)

* Correspondence: taochengan@nudt.edu.cn (C.-A.T.); wangjianfang@nudt.edu.cn (J.W.)

Abstract: Zr-containing metal-organic frameworks (MOFs) exhibit a good performance of catalyzing the hydrolysis of chemical warfare agents, which is closely related to the size of MOF particles and its defects, but these two factors are often intertwined. In this article, we synthesized UiO-66-NH$_2$ nanoparticles using a microwave-assisted hydrothermal method. By using a new modulator 4-Fluoro-3-Formyl-Benzoic Acid (FFBA) in different proportions, MOF particles with the same defect degree but different scales and those with similar sizes but different defect degrees can be obtained. The performance of the obtained MOF particles to catalyze the hydrolysis of the nerve agent simulant, dimethyl 4-nitrophenyl phosphate (DMNP), was investigated, and the effects of single factors of size or defect were compared for the first time. As the size of the obtained MOF particles increased from 81 nm to 159 nm, the catalytic degradation efficiency toward DMNP gradually decreased, and the half-life increased from 3.9 min to 11.1 min. For MOFs that have similar crystal sizes, the catalytic degradation half-life of MOF3 is only 5 min, which is much smaller than that of MOF5 due to the defects increase from 1.2 to 1.8 per Zr$_6$ cluster.

Keywords: metal-organic framework; zirconium; catalysis; microwave-assisted reaction; chemical warfare agent

1. Introduction

Chemical warfare agents (CWAs) containing phosphonate ester bonds, which are named nerve agents, such as GA (Tabun), GB (Sarin), and GD (Soman), are among the most toxic chemicals known to mankind [1]. Recently, a series of world events [2–5] have made it necessary to continue to study the rapid destruction of these forbidden CWAs. Hydrolysis-based decontamination of CWAs remains an important way. The key is to find suitable catalysts to accelerate this process. Metal-organic frameworks (MOFs) are organic-inorganic hybrid materials, which have well-organized pore structures. With the help of coordination bonds, MOFs can be assembled by metal ions or metal-oxygen clusters and organic bridging ligands [6,7]. Recently, benefiting from their excellent properties such as ordered and tunable pore sizes, high surface areas, abundant metal sites, and controllable chemistry microenvironment, certain MOFs have been demonstrated to be promising catalysts, which can catalyze the degradation of toxic nerve agents and their simulants (hydrolysis). They can even detoxify such a deadly substance in just a few minutes [8–11] by providing people with new protection against the threat of CWA.

The typical effective MOFs usually contain Zr$_6$ clusters, such as UiO-66 (Universitet of Oslo), UiO-66-NH$_2$, UiO-67, MOF-808, and NU-1000 [8–10]. They have multiple Zr-OH-Zr moieties, which can

potential mimic the Lewis-acidic Zn–OH–Zn active site found in G-agent destroying enzymes such as phosphotriesterase [5,12]. In addition, Zr-MOFs, like UiO-66-NH$_2$, can be used as an active material for the sensor to identify a trace nerve agent [13]. Previous reports have revealed that most MOFs containing the small sizes of the pore structure, which hinder the reactants to go inside the interior pores of MOF and lead to the reaction, are diffusion-limited and their catalysis mainly occurred on the external surface of MOF particles [14,15]. Therefore, the size of MOFs has an important effect on catalysis, and the smaller the size of MOF crystals is, the more specific surface area/catalytic sites are available [16,17]. The defects in MOFs, such as missing linkers or nodes, is another important factor for the hydrolysis reaction of CWAs [18]. These two factors are often intertwined. For example, Peterson et al. [19] introduced more defects to the UiO-66-NH$_2$. They found the high defect MOF (1.27 defects per node) has a reaction half-life by 20-fold shorter than that of a low defect MOF (0.55 defects per node). However, the high defect sample also have a significantly smaller crystal size than the smaller sample, which may contribute to enhance catalysis efficiency. Li et al. [17] reported the relationship between the catalytic hydrolysis of methyl paraoxon and the size of NU-1000 crystallites, and a remarkable increase in the rate was observed by reducing the crystal size. However, the defects in the MOFs were not discussed.

In this study, we try to synthesize UiO-66-NH$_2$ nanoparticles with the same defective degree but different sizes. 4-Fluoro-3-Formyl-Benzoic Acid (FFBA) with a molecular structure similar to that of organic linker, 2-Aminoterephthalic acid (BDC-NH$_2$), was used as a modulator, and a microwave-assisted solvothermal synthesis method was used to rapidly synthesize UiO-66-NH$_2$ particles (Scheme 1). As the proportion of modifier FFBA increases from 0:10 to 1:9, 5:5 (molar ratio of FFBA to BDC-NH$_2$), the size of MOF particles increases while keeping the defective degrees of the MOFs the same, which is equal to 1.2 per Zr$_6$ cluster. However, when the ratio of FFBA to BDC-NH$_2$ was fixed to 3:7, the defect of synthesized MOF (MOF**3**) increased to 1.8 per Zr6 cluster, while keeping the crystal size similar to that of MOF**5** obtained when the molar ratio of FFBA to BDC-NH$_2$ was 5:5. The performance of these obtained MOF particles to catalyze the hydrolysis of the nerve agent simulant, dimethyl 4-nitrophenyl phosphate (DMNP), was explored, and the effects of single factors of size or defect were discussed for the first time.
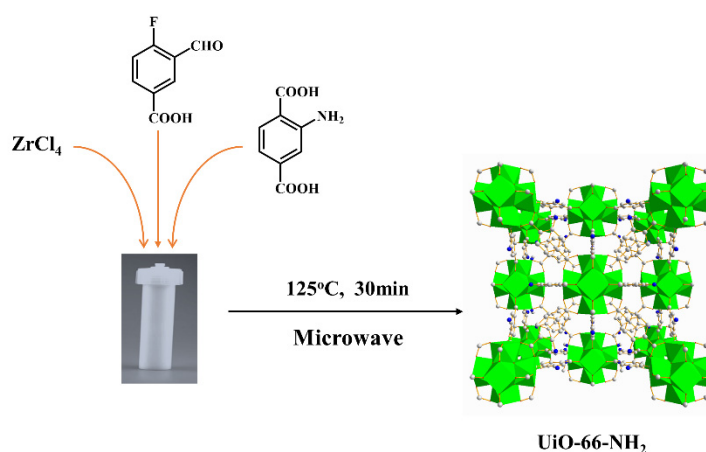
Scheme 1. Illustration for microwave-assisted solvothermal synthesis of UiO-66-NH$_2$ with 4-Fluoro-3-Formyl-Benzoic Acid (FFBA) as a modulator.

2. Results

2.1. Synthesis and Characterization of UiO-66-NH2

UiO-66-NH$_2$ was prepared by a microwave-assisted solvothermal method with a varied molar ratio of FFBA to BDC-NH$_2$ and the obtained solid products with the ratio of 10:0, 9:1, 7:3, and 5:5 were labelled as MOF**0**, MOF**1**, MOF**3**, and MOF**5**, respectively. In order to confirm the success of the

synthesis of UiO-66-NH$_2$, Powder X-ray diffraction (PXRD), Fourier transform infrared spectra (FT-IR), scanning electron microscope (SEM), thermogravimetric analyses (TGA), Nitrogen physisorption, and nuclear magnetic resonance spectrometry (NMR) were used for characterization. As shown in Figure 1, the X-ray diffraction (XRD) patterns of all the four synthesized MOFs agree well with the simulated patterns from UiO-66 cif file [20]. There are three characteristic diffraction peaks at 7.4°, 8.5°, and 25.8° corresponding to the (110), (200), and (600) planes of UiO-66-NH$_2$. As the molar ratio of BDC-NH$_2$ and FFBA varied, the MOF products have the very similar patterns. PXRD results prove the success of the synthesis of UiO-66-NH$_2$ with high crystallinity with or without the modulator of FFBA.
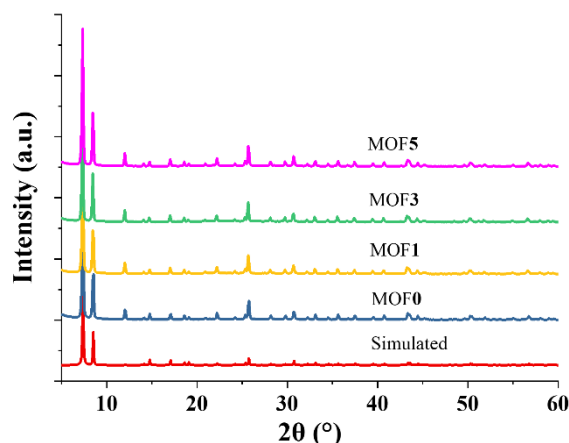

Figure 1. X-ray diffraction (XRD) patterns of the obtained metal organic framework (MOF) products.

The Fourier transform infrared (FT-IR) spectra of the produced MOFs and organic linker, NH$_2$-BDC, are shown in Figure 2. In the spectrum of NH$_2$-BDC, the vibrational bands around 3389 cm^{-1} and 3506 cm^{-1} correspond to (–NH$_2$) group, the broad band around 2500–3000 cm^{-1} ascribes to the coupled -OH of COOH, and the strong peak at 1682 cm^{-1} is assigned to the C=O stretching of COOH [21]. The spectra of MOF**0**, MOF**1**, MOF**3,** and MOF**5** are almost the same. The three strong peaks at 1567, 1427, and 1385 cm^{-1} originate from the carboxyl group on the organic linker, NH$_2$-BDC. The triplet peaks at 767, 663, and 482 cm^{-1} spring from O-Zr-O vibrations in the metal-oxygen clusters [22]. The broad band around 2500–3000 cm^{-1} disappears and no band at around 1680 is observed, which indicates all the (–COOH) in NH$_2$-BDC were coordinated with the Zr$_6$ cluster and all modulators (BBFA) are rinsed out completely.
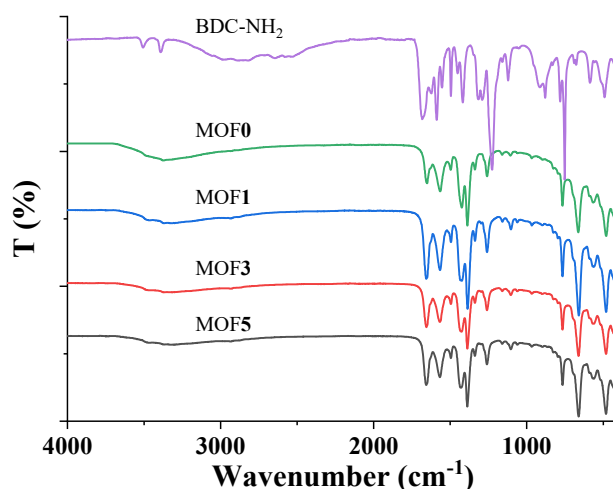

Figure 2. Fourier transform infrared spectra of the obtained MOF products.

Morphologies of produced MOFs were investigated by scanning electron microscopy (SEM) observation, and the results are shown in Figure 3. All samples exhibit well-shaped octahedral shapes, but the dispersion of their sizes using different amounts of the BBFA modulator is very broad. The size distribution of MOF**0**, MOF**1**, MOF**3**, and MOF**5** in Figure 3 were analyzed, as shown in Figures S1–S4. When no BBFA is added, the obtained UiO-66-NH$_2$ nanocrystals (MOF**0**) are uniform and small. The average size is 81.2 nm. When the ratio of BBFA to BDC-NH$_2$ increases to 1:9, the obtained MOF1 nanocrystals are slightly agglomerated. The average size of MOF**1** increases to 111.3 nm. When the ratio of BBFA to BDC-NH$_2$ further increases to 3:7, it can be observed that there are two different sizes of BDC-NH$_2$ particles generated. The smaller one is about 149.3 nm and the larger one is about 300 nm. When adding more modulator BBFA, up to one equivalent per BDC-NH$_2$, the obtained UiO-66-NH$_2$ nanocrystals (MOF**5**) become uniform again and the average size is about 159.3 nm.
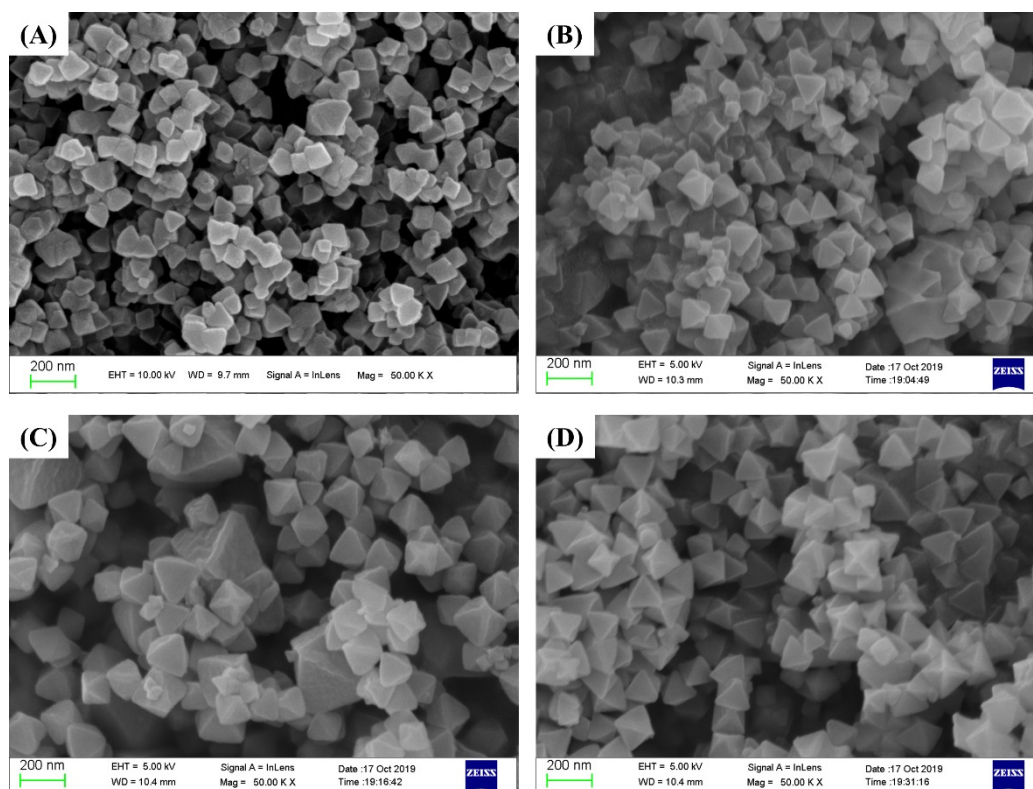

Figure 3. Scanning electron microscopy (SEM) images of the obtained MOF products. (**A**) MOF**0**, (**B**) MOF**1,** (**C**) MOF**3,** and (**D**) MOF**5**.

In addition, Lillerud's protocol [23] was used to confirm and evaluate the existence of defects from the thermogravimetric analysis (TGA) curves under air flow. The molecular weight of Zr$_6$O$_6$ (BDC-NH$_2$)$_6$, the dehydroxylated form of UiO-66-NH$_2$ is 2.32 times of 6ZrO$_2$, which is the only solid product after aerobic decomposition of UiO-66-NH$_2$. Therefore, if the final weight of the aerobic TGAoperation is normalized to 100%, the plateau (representing the empty, solvent-free material) should ideally reach 232%. The normalized TGA curves of the obtained MOFs were plotted in Figure 4. The weight of MOF**0**, MOF**1** and MOF**5** at 297 °C is almost similar, which is 203.3% of 6ZrO$_2$. The estimated density of missing-linker defects in MOF**0**, MOF**1**, and MOF**5** per Zr$_6$ cluster is only 1.2. Unexpectedly, the weight of MOF**3** at 297 °C is only 189.8% of 6ZrO$_2$, and the estimated defects of MOF**3** reaches as high as 1.8 per Zr$_6$ cluster.
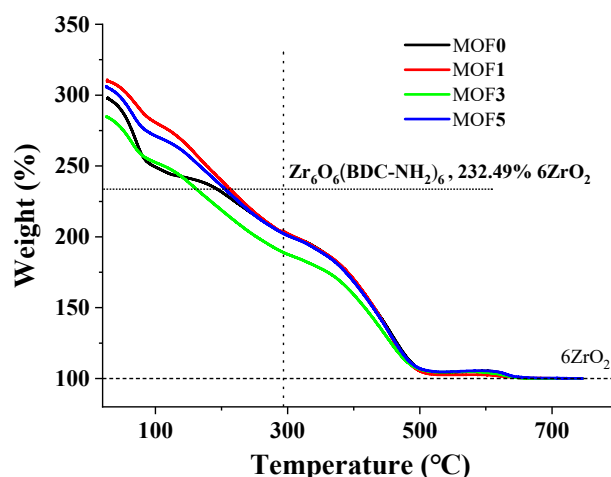
Figure 4. Thermogravimetric curves of the obtained MOF products.

The specific surface areas and pore structures were determined by Nitrogen adsorption-desorption isotherms, as shown in Figure 5. When p/p_0 is less than 0.01, the adsorption capacity rises linearly, which indicates that the samples contain a large number of micropores. As the relative pressure increases, the adsorption isotherm bends into a plateau. When p/p_0 increases to more than 0.9, the adsorption capacity increased significantly, which indicates that there is a certain macroporous structure in the sample. Combined with the SEM observation, it can be observed that the macropores are formed by accumulating MOF particles. The adsorption and desorption isotherm characteristics of the four samples are very similar, which indicates that their pore structure characteristics are almost the same. The Brunauer-Emmett-Teller (BET) specific surface areas of MOF**0**, MOF**1**, MOF**3**, and MOF**5** are 642.9, 679.7, 691.3, and 741.2 m^2/g, respectively, that is, with the increase of the modulator FFBA, the specific surface area slightly increases. Furthermore, the pore size distribution of the four were analyzed by Horvath–Kawazoe (HK) and Barrett-Joyner-Halenda (BJH) methods, and the results are presented in Figures S5–S8 and S9–S12, respectively. In the micropore range (<2 nm), the most probable pore size distribution of the four samples is about 0.5 nm (Figures S5–S8), which is very close to the theoretical dynamic pore size of UiO-66-NH$_2$. In the mesoporous range (2–50 nm) and macroporous range (>50 nm) (Figures S9–S12), the four samples have no clear pore distribution, which indicates that the defect degree is not high enough, and the defect-induced pores are not clear.
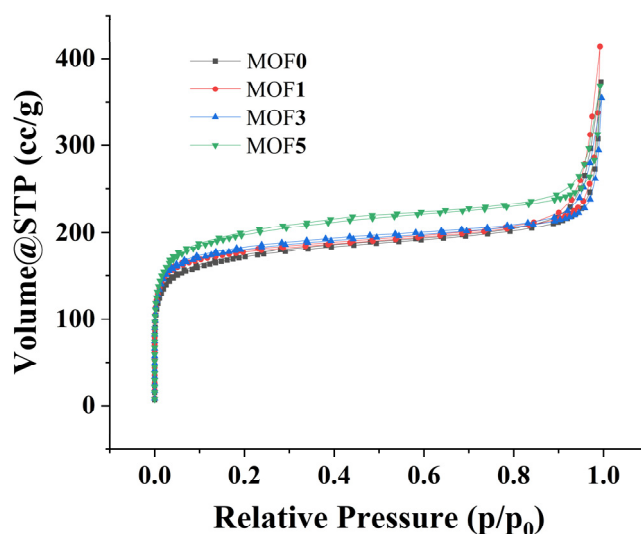

Figure 5. Nitrogen adsorption-desorption isotherms of the obtained MOF products.

As we know, in some cases, the modulator can coordinate to the cluster (especially in defective structures) in the synthesis process. In this case, we use NMR spectra to confirm if the new modulator FFBA would coordinate to the Zr_6 cluster. The ^{19}F, ^1H, and ^{13}C NMR spectra of four obtained MOF samples were performed and those spectra of FFBA, BDC-NH_2, and DMF were also carried out for comparison. Figure S13 exhibits the chemical structures of DMF, BDC-NH_2, and FFBA in the NMR test when $NaOD/D_2O$ (10 wt%) was used as the solvent. The ^{19}F spectra (Figure S14) clearly show that the four MOF samples do not contain the FFBA modulator. The ^1H and ^{13}C spectra (Figures S15 and S16) further confirms this conclusion. They suggest that the four MOF samples contain only BDC-NH_2 ligands besides a small amount of residual DMF.

2.2. Catalysis Performance toward the Hydrolysis of DMNP

To determine the catalytic performance of obtained UiO-66-NH_2 toward the detoxification of CWAs, the catalysis on the hydrolysis of the CWA simulant, DMNP, was investigated for safety. DMNP has been widely used to simulate GA (Tabun), GB (Sarin), and GD (Soman) nerve agents [15,24] because they all contain similar phosphate ester bonds, but DMNP has much lower toxicity. Another advantage of using DMNP is that its decomposition product, 4-nitrophenol (Scheme 2) [6,7], has an absorption peak at around 407 nm, which makes it very easy to monitor the reaction process by Ultraviolet-visible (UV-Vis) spectroscopy.
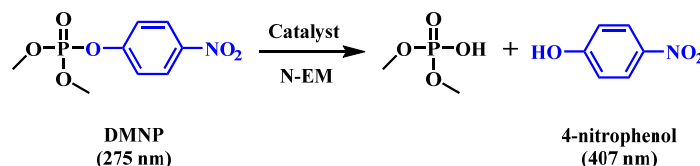
Scheme 2. Degradation of dimethyl 4-nitrophenyl phosphate (DMNP) to 4-nitrophenol.

The observed UV-vis spectra of hydrolysis reaction for DMNP using MOF**0** as a catalyst were shown in Figure 6A, the intensity at 275 nm (corresponding to DMNP) decreases, and the peak at 407 nm (corresponding to 4-nitrophenol) increases along with time, which indicates that the DMNP can be effectively degraded and 4-nitrophenol can be released in the presence of MOF**0**. The monitor UV-vis spectra of the hydrolysis reaction of DMNP in the presence of MOF**1**, MOF**3**, and MOF**5** were shown in Figures S17–S19. The conversion profiles were further calculated and are given in Figure 6B. The half-lives of hydrolysis of DMNP were evaluated, according to first-order kinetics (Figures S20–S23), and are presented in Table 1. The MOF**0** shows high efficiency in hydrolyzing DMNP. The half-life of DMNP hydrolysis with MOF**0** as a catalyst is 3.9 min, and, after 20 min, the hydrolysis rate can appear up to 90%. The half-lives of DMNP hydrolysis with MOF**1**, MOF**3**, and MOF**5** as catalysts are 9.1, 5.0, and 11.1 min, respectively. The half-life of DMNP hydrolysis with no catalysts is as long as 1634 min, which suggests that all of the obtained UiO-66-NH_2 can effectively catalyze DMNP to hydrolysis.
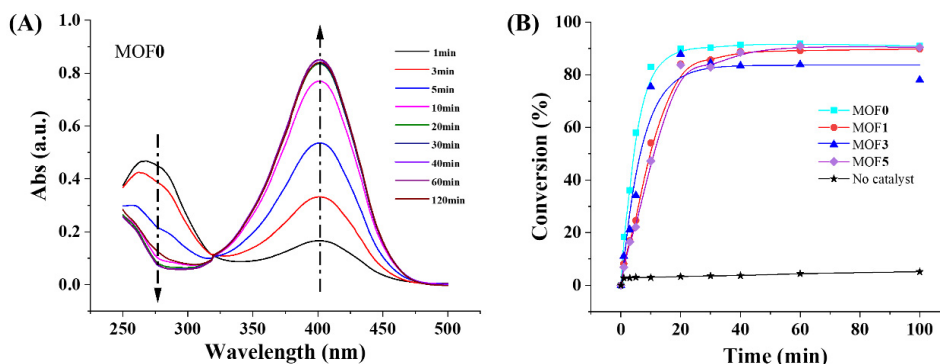

Figure 6. (**A**) Hydrolysis reaction for DMNP using MOF**0** as a catalyst, (**B**) conversion for the hydrolysis of DMNP in the presence of MOF**0**, MOF**1**, MOF**3**, and MOF**5** or without catalysts.

Table 1. Catalytic performance of obtained products for degrading the nerve agent Simulant DMNP.

Sample	Size (nm)	Defects	k_1 (min^{-1})	$t_{1/2}$ (min)
MOF**0**	81.2	1.2	0.177	3.9
MOF**1**	111.3	1.2	0.076	9.1
MOF**3**	149.3, 300	1.8	0.139	5.0
MOF**5**	159.3	1.2	0.062	11.1
No catalyst	-	-	4.2×10^{-4}	1634

3. Discussion

The three-dimensional relationship diagram of the first-order chemical reaction rate constant (k_1) with the sizes of the MOF catalysts and their defect degrees were shown in Figure 7. MOF**0**, MOF**1**, and MOF**5** have a very similar defect degree estimated from the TGA curve, while they have different sizes. MOF**0** is only about 81.2 nm, MOF**1** increases to 111.3 nm, and MOF**5** is as large as 159.3 nm. Accordingly, the calculated first-order chemical reaction rate constants (k_1) of the hydrolysis reaction of DMNP with MOF**0**, MOF**1,** or MOF**5** as catalysts are 0.177, 0.076, and 0.062 min^{-1}, respectively. It indicates that the catalytic performance of MOF particles is inversely proportional to the size of MOF particles, when the defect density is equal. For MOF**3**, most of them are relatively small particles with a size of 149.3 nm, and a small number of particles at around 300 nm. Comparing MOF**3** and MOF**5**, they have similar sizes, but their defect density is very different. MOF**3** reaches 1.8 per Zr$_6$ unit, while MOF**5** only has 1.2 per Zr$_6$ cluster. Comparing the catalytic performance of the two, it can be seen that the reaction rate constant of MOF**3** is 122% higher than that of MOF**5**, and the half-life is only 45% of that of MOF**5**, which is as short as about 5 min. This is almost comparable to that of MOF**0**. The result testifies that the defects of MOFs play an important role in catalyzing the decomposition of DMNP. The greater the degree of MOF defects, the better the catalytic performance of MOF.
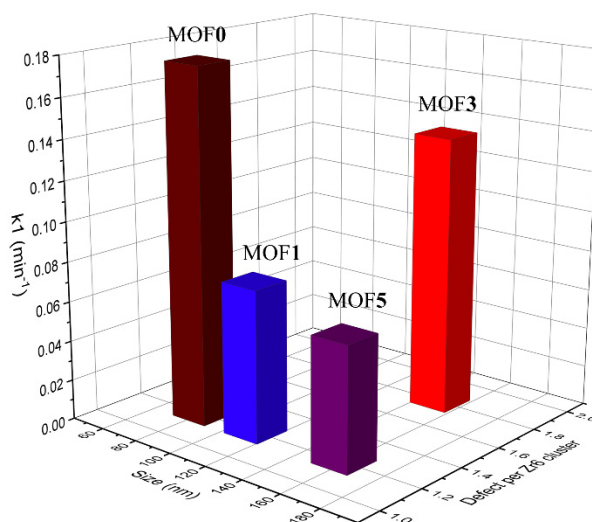
Figure 7. The three-dimensional relationship diagram of the first-order chemical reaction rate constant (k_1) with the sizes of the MOF catalysts and their defect degrees.

It is worth mentioning that there have been several reports concerning the degradation properties of UiO-66-NH$_2$ powders [19,25–30]. The shortest half-life of degradation of DMNP catalyzed by UiO-66-NH$_2$ reported in the literature is less than 1 min [26] while the longest half-life reaches 495 min [19]. This difference is mainly due to the different sizes of MOF catalyst particles and the introduction of different defects. However, these two factors are often intertwined with each other, and there is no sufficient direct investigation of the influence of a single factor in the previous literature when the other factor is the same. Herein, the UiO-66-NH$_2$ nanoparticles with different sizes and the

same defects were produced. The particles with different defects and similar sizes were also obtained in the same procedure with different ratios of modulator BBFA to BDC-NH$_2$. The effect of a single factor of size or defect was discussed directly for the first time. The kinetic parameters of DMNP hydrolysis catalyzed different Zr-MOFs reported in the literatures are listed in Table S1. Besides UiO-66-NH$_2$, other Zr-based MOFs, such as UiO-66 [15], UiO-67 [31], NU-1000 [12], and MOF-808 [32], were also explored for catalyzing the hydrolysis of nerve agent simulants. Typical half-lives of UiO-66 and NU-1000 are 35 min and 15 min, respectively, which were longer than that of those MOFs obtained in this scenario. In addition, the half-life of UiO-67 are about 3.5 min, which is comparable with those reported in this case. Furthermore, the half-lives of dehydrated NU-1000 and MOF-808 are only 1.5 min and 0.5 min, which are shorter than those reported in this work. Further optimization of the defect degree and particle size of UiO-66-NH$_2$ is expected to further improve its catalytic performance, reaching, or even exceeding, the catalytic activity of dehydrated NU-1000 and MOF-808.

4. Materials and Methods

4.1. Materials

Anhydrous zirconium (IV) chloride (ZrCl$_4$) was obtained from Acros Organics (Janssens Pharmaceuticalaan 3A, Geel, Belgium). BDC-NH$_2$ was purchased from Alfa Aesar (China) Chemical (Shanghai, China). FFBA was supplied by Adamas Chemical (Shanghai, China). N-ethylmorpholine (N-EM) were purchased from Macklin Chemical (Shanghai, China). DMNP was home-made. All chemicals were used as received with no further purification.

4.2. Synthesis of UiO-66-NH$_2$

UiO-66-NH$_2$ was synthesized by microwave-assisted solvothermal method according to literature with modification [33–35]. Typically, ZrCl$_4$ (320 mg, 1.37 mmol) was dissolved in 50 mL DMF in a 200-mL beaker. Then 7-mL acetic acid (HAc) and 286-μl concentrated hydrochloric acid (HCl) were added into the solution. Afterward, a total of 1.38 mmol of BDC-NH$_2$ ligand and FFBA modulator were added into the mixture. The molar ratio of BDC-NH$_2$ and FFBA was varied to be 10:0, 9:1, 7:3, and 5:5, respectively. The mixture was transferred into a Teflon autoclave after 30 min of stirring. Furthermore, the autoclave was heated to 125 °C in a XH-300-A+ microwave reactor (Xianghu, Beijing) with an irradiation power of 300 W and kept there for 30 min. After cooling to room temperature, the synthesized products were obtained by centrifugation (12000 rpm), washing (2 times in DMF, soaking in acetone overnight), and drying (120 °C).

4.3. Catalytic Degration of DMNP

Catalytic hydrolysis of DMNP was performed according to the previous reports [29,30]. Typically, 10.4 mg of catalyst (MOF**0**, MOF**1**, MOF**3**, and MOF**5**, respectively) was added to 4.0 mL of N-EM solution (0.45 M, pH = 10) in a 50-mL vial at 25 °C. The resulting dispersion was vigorously sonicated for 5 min and stirred at 1100 rpm for 5 min. Then, 16 μL of DMNP was added to the suspension, and the stirring was kept at 1100 rpm. A 20-μL aliquot from the reaction mixture was taken out at a specific time, and diluted with 10 mL of N-EM solution (0.45 M). Catalytic efficiency was evaluated by observing the absorbance at 407 nm of 4-nitrophenoxide. For comparison, similar experiments were performed without a catalyst.

4.4. Characterization

PXRD patterns of the obtained MOFs were measured on a diffractometer (Bruker D8, Karlsruhe, Germany) with Cu Ka = 1.5418 Å. FT-IR were obtained using a spectrometer (Spectrum-Two, PerkinElmer, Waltham, MA, USA) equipped with an attenuated total reflectance (ATR) accessory. SEM images were observed on a Zeiss Sigma HD microscope (Jena, Japan). TGA were carried out on a thermal analyzer (STA6000, PerkinElmer, Waltham, MA, USA) under air flow at a heating

rate of 10 °C/min. Nitrogen adsorption-desorption isotherms were recorded from a Quantachrome AUTOSORB IQ analyzer (Boynton Beach, FL, USA). NMR spectra were acquired on a Bruker 400M NMR spectrometer (Ettlingen, Germany). UV-Vis spectroscopy monitoring of DMNP hydrolysis in the range of 250–500 nm was performed using a spectrophotometer (LabTech BlueStarA, Beijing, China).

5. Conclusions

In this work, we have successfully prepared UiO-66-NH$_2$ using a rapid microwave-assisted solvothermal method. A new modulator of BBFA whose structure is similar to the ligand can effectively regulate the crystal size and defects of UiO-66-NH$_2$. The UiO-66-NH$_2$ nanoparticles with different sizes and the same defects as well as particles with different defects and similar sizes can be produced in the same procedure with different ratios of modulator BBFA to BDC-NH$_2$. Benefiting from this, the effect of a single factor of size or defect have been discussed directly for the first time. The catalytic performance of MOF particles is inversely proportional to the size of MOF particles when the defect density is equal. Furthermore, the greater the degree of MOF defects is, the better the catalytic performance of MOF is. Therefore, the preparation of MOF with both a small size and high defects is an important way to improve its catalytic performance.

References

1. Üzümcü, A. The chemical weapons convention—Disarmament, science and technology. *Anal. Bioanal. Chem.* **2014**, *406*, 5071–5073. [CrossRef]
2. Bobbitt, N.S.; Mendonca, M.L.; Howarth, A.J.; Islamoglu, T.; Hupp, J.T.; Farha, O.K.; Snurr, R.Q. Metal-organic frameworks for the removal of toxic industrial chemicals and chemical warfare agents. *Chem. Soc. Rev.* **2017**, *46*, 3357–3385. [CrossRef] [PubMed]
3. Yusof, M.N. *Statement by H.E. Ambassador Ahmad Nazri Yusof Perminant Representative of Malaysia to the OPCW*; OPCW: The Hague, The Netherlands, 2017.
4. Wilson, P. *Statement by HE Ambassador Peter Wilson Perminant Representative of the United Kingdom of Great Britian and Northern Ireland to the OPCW*; OPCW: The Hague, The Netherlands, 2018.
5. Bigley, A.N.; Raushel, F.M. The evolution of phosphotriesterase for decontamination and detoxification of organophosphorus chemical warfare agents. *Chem. Biol. Interact.* **2019**, *308*, 80–88. [CrossRef] [PubMed]
6. Stock, N.; Biswas, S. Synthesis of Metal-Organic Frameworks (MOFs): Routes to Various MOF Topologies, Morphologies, and Composites. *Chem. Rev.* **2012**, *112*, 933–969. [CrossRef] [PubMed]
7. Zhou, H.; Long, J.R.; Yaghi, O.M. Introduction to Metal–Organic Frameworks. *Chem. Rev.* **2012**, *112*, 673–674. [CrossRef] [PubMed]
8. Vellingiri, K.; Philip, L.; Kim, K.H. Metal–organic frameworks as media for the catalytic degradation of chemical warfare agents. *Coordination Chem. Rev.* **2017**, *353*, 159–179. [CrossRef]
9. Mondal, S.S.; Holdt, H.-J. Breaking Down Chemical Weapons by Metal-Organic Frameworks. *Angew. Chem. Int. Ed.* **2016**, *55*, 42–44. [CrossRef]

10. Liu, Y.; Howarth, A.J.; Vermeulen, N.A.; Moon, S.-Y.; Hupp, J.T.; Farha, O.K. Catalytic degradation of chemical warfare agents and their simulants by metal-organic frameworks. *Coord. Chem. Rev.* **2017**, *346*, 101–111. [CrossRef]

11. De Koning, M.C.; Van Grol, M.; Breijaert, T. Degradation of Paraoxon and the Chemical Warfare Agents VX, Tabun, and Soman by the Metal–Organic Frameworks UiO-66-NH2, MOF-808, NU-1000, and PCN-777. *Inorg. Chem.* **2017**, *56*, 11804–11809. [CrossRef]

12. Mondloch, J.E.; Katz, M.J.; Isley, W.C.; Ghosh, P.; Liao, P.; Bury, W.; Wagner, G.W.; Hall, M.G.; Decoste, J.B.; Peterson, G.W. Destruction of chemical warfare agents using metal–organic frameworks. *Nat. Mater.* **2015**, *14*, 512–516. [CrossRef]

13. Stassen, I.; Bueken, B.; Reinsch, H.; Oudenhoven, J.F.M.; Wouters, D.; Hajek, J.; Van Speybroeck, V.; Stock, N.; Vereecken, P.M.; Van Schaijk, R. Towards metal–organic framework based field effect chemical sensors: UiO-66-NH2 for nerve agent detection. *Chem. Sci.* **2016**, *7*, 5827–5832. [CrossRef] [PubMed]

14. Wang, G.; Sharp, C.; Plonka, A.M.; Wang, Q.; Frenkel, A.I.; Guo, W.; Hill, C.; Smith, C.; Kollar, J.; Troya, D.; et al. Mechanism and Kinetics for Reaction of the Chemical Warfare Agent Simulant, DMMP(g), with Zirconium(IV) MOFs: An Ultrahigh-Vacuum and DFT Study. *J. Phys. Chem. C* **2017**, *121*, 11261–11272. [CrossRef]

15. Katz, M.J.; Mondloch, J.E.; Totten, R.K.; Park, J.K.; Nguyen, S.T.; Farha, O.K.; Hupp, J.T. Simple and Compelling Biomimetic Metal-Organic Framework Catalyst for the Degradation of Nerve Agent Simulants. *Angew. Chem. Int. Ed.* **2014**, *53*, 497–501. [CrossRef] [PubMed]

16. Cho, K.Y.; Seo, J.Y.; Kim, H.-J.; Pai, S.J.; Do, X.H.; Yoon, H.G.; Hwang, S.S.; Han, S.S.; Baek, K.-Y. Facile control of defect site density and particle size of UiO-66 for enhanced hydrolysis rates: Insights into feasibility of Zr(IV)-based metal-organic framework (MOF) catalysts. *Appl. Catal. B-Environ.* **2019**, *245*, 635–647. [CrossRef]

17. Li, P.; Klet, R.C.; Moon, S.; Wang, T.C.; Deria, P.; Peters, A.W.; Klahr, B.M.; Park, H.J.; Aljuaid, S.S.; Hupp, J.T. Synthesis of nanocrystals of Zr-based metal–organic frameworks with csq-net: Significant enhancement in the degradation of a nerve agent simulant. *Chem. Commun.* **2015**, *51*, 10925–10928. [CrossRef] [PubMed]

18. Harvey, J.A.; Greathouse, J.A.; Gallis, D.F.S. Defect and Linker Effects on the Binding of Organophosphorous Compounds in UiO-66 and Rare-Earth MOFs. *J. Phys. Chem. C* **2018**, *122*, 26889–26896. [CrossRef]

19. Peterson, G.W.; Destefano, M.R.; Garibay, S.J.; Ploskonka, A.M.; Mcentee, M.; Hall, M.G.; Karwacki, C.J.; Hupp, J.T.; Farha, O.K. Optimizing Toxic Chemical Removal through Defect-Induced UiO-66-NH2 Metal–Organic Framework. *Chem. A Eur. J.* **2017**, *23*, 15913–15916. [CrossRef]

20. Katz, M.J.; Brown, Z.J.; Colon, Y.J.; Siu, P.W.; Scheidt, K.A.; Snurr, R.Q.; Hupp, J.T.; Farha, O.K. A facile synthesis of UiO-66, UiO-67 and their derivatives. *Chem. Commun.* **2013**, *49*, 9449–9451. [CrossRef]

21. Karthikeyan, N.; Joseph Prince, J.; Ramalingam, S.; Periandy, S. Electronic [UV–Visible] and vibrational [FT-IR, FT-Raman] investigation and NMR–mass spectroscopic analysis of terephthalic acid using quantum Gaussian calculations. *Spectrochim. Acta Part A Mol. Biomol. Spectrosc.* **2015**, *139*, 229–242. [CrossRef]

22. Cavka, J.H.; Jakobsen, S.; Olsbye, U.; Guillou, N.; Lamberti, C.; Bordiga, S.; Lillerud, K.P. A new zirconium inorganic building brick forming metal organic frameworks with exceptional stability. *J. Am. Chem. Soc.* **2008**, *130*, 13850–13851. [CrossRef]

23. Shearer, G.C.; Chavan, S.; Ethiraj, J.; Vitillo, J.G.; Svelle, S.; Olsbye, U.; Lamberti, C.; Bordiga, S.; Lillerud, K.P. Tuned to Perfection: Ironing Out the Defects in Metal–Organic Framework UiO-66. *Chem. Mater.* **2014**, *26*, 4068–4071. [CrossRef]

24. Ploskonka, A.M.; Decoste, J.B. Insight into Organophosphate Chemical Warfare Agent Simulant Hydrolysis in Metal-Organic Frameworks. *J. Hazard. Mater.* **2019**, *375*, 191–197. [CrossRef] [PubMed]

25. Islamoglu, T.; Ortuño, M.A.; Proussaloglou, E.; Howarth, A.J.; Vermeulen, N.A.; Atilgan, A.; Asiri, A.M.; Cramer, C.J.; Farha, O.K. Presence versus Proximity: The Role of Pendant Amines in the Catalytic Hydrolysis of a Nerve Agent Simulant. *Angew. Chem. Int. Ed.* **2018**, *57*, 1949–1953. [CrossRef] [PubMed]

26. Peterson, G.W.; Moon, S.; Wagner, G.W.; Hall, M.G.; Decoste, J.B.; Hupp, J.T.; Farha, O.K. Tailoring the Pore Size and Functionality of UiO-Type Metal–Organic Frameworks for Optimal Nerve Agent Destruction. *Inorg. Chem.* **2015**, *54*, 9684–9686. [CrossRef]

27. Lu, A.X.; McEntee, M.; Browe, M.A.; Hall, M.G.; DeCoste, J.B.; Peterson, G.W. MOFabric: Electrospun Nanofiber Mats from PVDF/UiO-66-NH2 for Chemical Protection and Decontamination. *Acs Appl. Mater. Interfaces* **2017**, *9*, 13632–13636. [CrossRef]

28. Lee, D.T.; Zhao, J.; Peterson, G.W.; Parsons, G.N. Catalytic "MOF-Cloth" Formed via Directed Supramolecular Assembly of UiO-66-NH2 Crystals on Atomic Layer Deposition-Coated Textiles for Rapid Degradation of Chemical Warfare Agent Simulants. *Chem. Mater.* **2017**, *29*, 4894–4903. [CrossRef]

29. Chen, R.; Tao, C.-a.; Zhang, Z.; Chen, X.; Liu, Z.; Wang, J. Layer-by-layer Fabrication of Core-Shell Fe3O4@UiO-66-NH2 with High Catalytic Reactivity toward the Hydrolysis of Chemical Warfare Agent Simulants. *ACS Appl. Mater. Interfaces* **2019**, *11*, 43156–43165. [CrossRef]

30. Shen, C.; Mao, Z.; Xu, H.; Zhang, L.; Zhong, Y.; Wang, B.; Feng, X.; Tao, C.-a.; Sui, X. Catalytic MOF-loaded cellulose sponge for rapid degradation of chemical warfare agents simulant. *Carbohydr. Polym.* **2019**, *213*, 184–191. [CrossRef]

31. Katz, M.J.; Moon, S.; Mondloch, J.E.; Beyzavi, M.H.; Stephenson, C.J.; Hupp, J.T.; Farha, O.K. Exploiting parameter space in MOFs: A 20-fold enhancement of phosphate-ester hydrolysis with UiO-66-NH2. *Chem. Sci.* **2015**, *6*, 2286–2291. [CrossRef]

32. Moon, S.-Y.; Liu, Y.; Hupp, J.T.; Farha, O.K. Instantaneous Hydrolysis of Nerve-Agent Simulants with a Six-Connected Zirconium-Based Metal-Organic Framework. *Angew. Chem. Int. Ed.* **2015**, *54*, 6795–6799. [CrossRef]

33. Huang, A.; Wan, L.; Caro, J. Microwave-assisted synthesis of well-shaped UiO-66-NH2 with high CO2 adsorption capacity. *Mater. Res. Bull.* **2018**, *98*, 308–313. [CrossRef]

34. Schaate, A.; Roy, P.; Godt, A.; Lippke, J.; Waltz, F.; Wiebcke, M.; Behrens, P. Modulated Synthesis of Zr-Based Metal–Organic Frameworks: From Nano to Single Crystals. *Chem. A Eur. J.* **2011**, *17*, 6643–6651. [CrossRef] [PubMed]

35. Schoenecker, P.M.; Belancik, G.A.; Grabicka, B.E.; Walton, K.S. Kinetics Study and Crystallization Process Design for Scale-Up of UiO-66-NH2 Synthesis. *AIChE J.* **2013**, *59*, 1255–1262. [CrossRef]